5

Shocks

In Chapter 4 we introduced the concept of shock waves. There we discussed how, when a fluid or plasma is set into motion at a particular spatial position by a pressure pulse that increases with time, the resulting acceleration can be approximated as a sequence of small velocity jumps. Each small jump in velocity launches a compression wave that travels into the fluid or plasma at the local adiabatic sound speed. As the pressure and hence the fluid velocity increases, each successive compression wave that is launched travels faster than the one before. Eventually all these compression waves "pile up," forming a single wave, a shock wave, that has a narrow wave front. The wave front is simply the narrow spatial region over which the flow variables transition from the undisturbed state ahead of the wave and the compressed state behind the wave.

In Chapter 1 we learned that one of the principal ways we create matter at extreme conditions in the laboratory is by dynamically compressing it with shock waves created by a "driver" like a high-power laser, a Z-pinch, or a gas-gun projectile. Shock physics is at the very heart of the simulation codes for describing the properties and behavior of matter at extreme conditions. Shocks also occur in nature. One example is the shock created in the gravitational collapse of a massive star at the end of its hydrogen-burning lifetime. It is this shock that ejects the envelope of the star into space that we see as a supernova explosion. Shocks play a prominent role also in the physics of astrophysical jet formation, in accretion processes, and in cosmic ray acceleration.

The objective in this chapter is to learn about the properties and behavior of shock waves. We start by deriving the relations between the flow variables ahead of and behind the shock front from the equations of motion – the conservation equations – that we derived in the previous chapter. Then, we will discuss some important properties of shock waves; introduce the concepts of entropy and adiabaticity as they apply to shock waves; and discuss the role of viscosity in defining the structure and width of the shock wave front. Then we will discuss the physics of blast waves,

which are shock waves in the atmosphere, and shocks in solids. We will also discover how shocks reduce to the isentropic compression waves we discussed in the last chapter in the limit of vanishing shock strength.

5.1 Rankine–Hugoniot equations

5.1.1 Jump conditions

Let us look again at Figure 4.2. In that figure we show schematically the flow variables on either side of a compression wave front, at position x_s, created by the push of a constant-velocity piston. In the figure we show the wave front as a discontinuity in the flow. We derived the conservation equations in Chapter 4 under the assumption that the flow is continuous everywhere, but that assumption is, in general, not necessary for the validity of the conservation relations. From a mathematical point of view, a discontinuity can be regarded as the limit of very large but finite gradients in the flow variables across a transition layer, the wave front, whose thickness goes to zero. In the limit of vanishing thickness, the wave front becomes a discontinuity. Thus, the conservation equations apply across the entire flow, continuous or discontinuous. For now, we will represent the shock front as a discontinuity in the flow. Thus, we can ignore the dissipation processes that take place in the shock front, and which define its thickness, and just apply the conservation equations to relate the flow variables behind the shock front to those in front of it.

Let us begin by rewriting the 1D equations of the conservation of mass, momentum, and energy we derived in the previous chapter, equations (4.7), (4.8), and (4.9):

$$\frac{\partial \rho}{\partial t} = -\frac{\partial}{\partial x}(\rho u), \tag{5.1}$$

$$\frac{\partial}{\partial t}(\rho u) = -\frac{\partial}{\partial x}\left(P + \rho u^2\right), \tag{5.2}$$

$$\frac{\partial}{\partial t}\left(\rho\varepsilon + \rho\frac{u^2}{2}\right) = -\frac{\partial}{\partial x}\left[\rho u\left(\varepsilon + \frac{u^2}{2} + \frac{P}{\rho}\right)\right]. \tag{5.3}$$

In equation (5.3) we have decomposed the total specific energy ε of equation (4.9) into the internal specific energy and the specific kinetic energy, that is, $\varepsilon \rightarrow \varepsilon + u^2/2$.

As discussed above, we now consider the shock discontinuity as a very thin layer between x_0 and x_1 in which the flow variables transition, with very large gradients, from their values ahead of the shock front, designated with the subscript 0, to their values behind the shock front, designated with the subscript 1. Then we integrate

the three conservation equations over this thin layer. For example, equation (5.1) becomes

$$\int_{x_0}^{x_1} \frac{\partial \rho}{\partial t} dx = -\int_{x_0}^{x_1} \frac{\partial}{\partial x} (\rho u)\, dx. \tag{5.4}$$

Similar integral equations can be written for the other two conservation equations. We then take the limit as the layer thickness goes to zero. The integrals on the left-hand side of these equations, being proportional to the layer thickness $x_1 - x_0$, go to zero as the layer thickness goes to zero. This is simply a mathematical way of saying that there is no accumulation of mass, momentum, or energy in the layer.

The integrals on the right-hand side of these equations give the differences between the flow variables on either side of the discontinuity. Thus, integrating equation (5.4) and taking the limit as the layer thickness vanishes, we get

$$\rho_1 u_1 = \rho_0 u_0. \tag{5.5}$$

In the same way we can derive the relations between the flow variables on either side of the shock discontinuity from the other two conservation equations, equations (5.2) and (5.3):

$$P_1 + \rho_1 u_1^2 = P_0 + \rho_0 u_0^2, \tag{5.6}$$

$$\varepsilon_1 + \frac{P_1}{\rho_1} + \frac{u_1^2}{2} = \varepsilon_0 + \frac{P_0}{\rho_0} + \frac{u_0^2}{2}. \tag{5.7}$$

The specific enthalpy is defined as

$$h = \varepsilon + \frac{P}{\rho}. \tag{5.8}$$

Using equation (5.8), we can rewrite equation (5.7) as

$$h_1 + \frac{u_1^2}{2} = h_0 + \frac{u_0^2}{2}. \tag{5.9}$$

Equations (5.5), (5.6), and (5.7) [or (5.9)] relate the four flow variables behind the shock discontinuity – u_1, ρ_1, P_1, and ε_1 (or h_1) – to the four flow variables in front of it – u_0, ρ_0, P_0, and ε_0 (or h_0). Thus, assuming we know (1) the pressure and density ahead of the shock, P_0 and ρ_0; (2) the equation of state of the fluid, $\varepsilon = \varepsilon(P, \rho)$ [or $h = h(P, \rho)$]; and (3) some parameter relating to the strength of the shock – for example, the pressure P_1 behind the shock, or the velocity of the "piston" push creating the shock, $u = u_0 - u_1$ – then we can solve the set of equations for all the flow variables behind the shock discontinuity.

First, we combine equations (5.5) and (5.6) to obtain:

$$u_0^2 = \mathcal{V}_0^2 \frac{P_1 - P_0}{\mathcal{V}_0 - \mathcal{V}_1}, \tag{5.10}$$

$$u_1^2 = \mathcal{V}_1^2 \frac{P_1 - P_0}{\mathcal{V}_0 - \mathcal{V}_1}. \tag{5.11}$$

The specific volume is defined as $\mathcal{V} \equiv 1/\rho$. Now, we substitute equations (5.10) and (5.11) into the energy conservation equation, equation (5.7), to obtain

$$\varepsilon_1 - \varepsilon_0 = \frac{1}{2}(P_1 + P_0)(\mathcal{V}_0 - \mathcal{V}_1). \tag{5.12}$$

Substituting enthalpies for energies, as per equation (5.8), we can rewrite equation (5.12) as

$$h_1 - h_0 = \frac{1}{2}(P_1 - P_0)(\mathcal{V}_0 + \mathcal{V}_1). \tag{5.13}$$

The specific internal energy ε (and enthalpy h) is a function only of the material's density and pressure. This relationship between internal energy, pressure, and density is the material's equation of state, which we will discuss in more detail in the next chapter. The important point for our discussion here is that we can see from equation (5.12) [and equation (5.13)] that we can express the pressure behind the shock, P_1, as a function of three variables: the pressure and specific volume ahead of the shock and the specific volume behind the shock. Thus,

$$P_1 = H(\mathcal{V}_1, P_0, \mathcal{V}_0). \tag{5.14}$$

The function H is referred to as the shock Hugoniot. Note that the Hugoniot defines an infinite family of curves in pressure–volume (or pressure–density) space, with each individual curve containing the point $(P_0, \mathcal{V})$. Figure 5.1 shows the Hugoniot curve for aluminum starting at standard temperature and pressure, ignoring phase transitions. We will see how this curve is modified by phase transitions in the next chapter.

The Hugoniot curve does *not* describe the trajectory of the shock-compressed material in pressure–volume space as it is undergoing the shock compression. Rather, the Hugoniot curve describes a *locus of points* for the equilibrium pressure behind the shock for a given compression and for given initial conditions.

Finally, let us use equations (5.10) and (5.11) to write an equation for the difference in specific kinetic energy on either side of the shock discontinuity in a

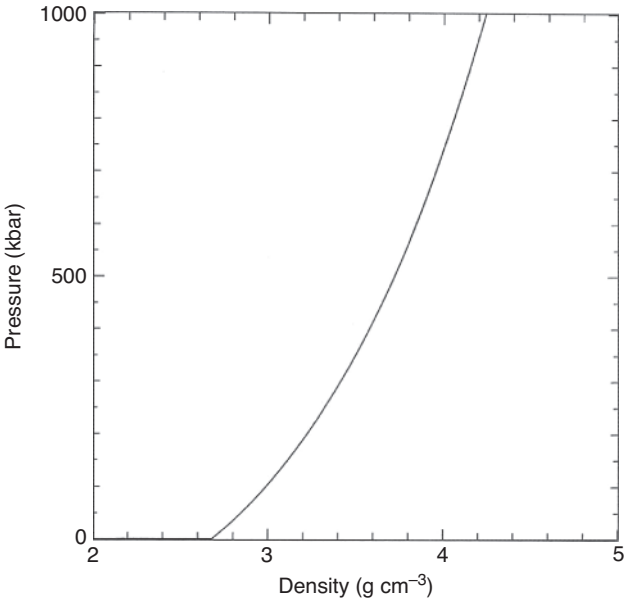

Figure 5.1 The Hugoniot curve for aluminum starting at standard temperature and pressure, ignoring phase transitions.

frame of reference in which the shock is at rest:

$$\frac{1}{2}\left(u_0^2 - u_1^2\right) = \frac{1}{2}\left(P_1 - P_0\right)\left(\mathcal{V}_0 + \mathcal{V}_1\right). \tag{5.15}$$

The right-hand side of equation (5.15) is identical to the right-hand side of equation (5.13). Thus, the change in specific kinetic energy of the material flowing through the shock discontinuity is equal to the change in the material enthalpy. In other words, some of the ordered motion of the particles is converted by the shock into random (thermal) motion. The stronger the shock, the greater this conversion.

5.1.2 Shocks in an ideal gas

For an equation of state that can be expressed with a simple analytic relationship, we can derive a simple analytic formula for the shock Hugoniot.

Let us, as an example, consider an ideal gas with constant specific heats. Consideration of shocks in an ideal gas can readily illuminate for us how the thermodynamic and flow variables change across the shock discontinuity.

We start by discussing the basic thermodynamic properties of an ideal gas. The generalized heat capacity of a substance is defined as dQ/dX, where Q is the specific heat energy and X is a thermodynamic variable. If $\varepsilon = \varepsilon(T, P)$ is the

https://doi.org/10.1017/CBO9781139095150.005 Published online by Cambridge University Press

specific internal energy and $\mathcal{V} = \mathcal{V}(T, P)$ the specific volume, then from the first law of thermodynamics we can write

$$dQ = \left(\frac{\partial \varepsilon}{\partial T}\bigg|_P + P \frac{\partial \mathcal{V}}{\partial T}\bigg|_P \right) dT + \left(\frac{\partial \varepsilon}{\partial P}\bigg|_T + P \frac{\partial \mathcal{V}}{\partial P}\bigg|_T \right) dP. \tag{5.16}$$

The first law of thermodynamics, $dQ = d\varepsilon + P d\mathcal{V}$, is simply a statement of conservation of energy; that is, the change in heat energy of any material is equal to its change in internal energy plus the work done in compressing it. For an isobaric path ($dP = 0$), we have the specific heat at constant pressure (also known as the isobaric heat capacity)

$$C_P \equiv \frac{\partial Q}{\partial T}\bigg|_P = \frac{\partial \varepsilon}{\partial T}\bigg|_p + P \frac{\partial \mathcal{V}}{\partial T}\bigg|_P. \tag{5.17}$$

Since $d\mathcal{V}$ is already an independent increment, we have only to express $d\varepsilon$ in terms of dT and $d\mathcal{V}$ and substitute the result into the first law. This gives

$$dQ = \frac{\partial \varepsilon}{\partial T}\bigg|_{\mathcal{V}} dT + \left[\frac{\partial \varepsilon}{\partial \mathcal{V}}\bigg|_T + P \right] d\mathcal{V}, \tag{5.18}$$

and for a constant volume change, we find the specific heat at constant volume (also known as the isochoric heat capacity)

$$C_V \equiv \frac{\partial Q}{\partial T}\bigg|_{\mathcal{V}} = \frac{\partial \varepsilon}{\partial T}\bigg|_{\mathcal{V}}. \tag{5.19}$$

Equating equation (5.16) to equation (5.18) we see that

$$C_P dT + L_P dP = C_V dT + \mathcal{V} d\mathcal{V}, \tag{5.20}$$

where L_P and L_V are latent heats. Now $d\mathcal{V} = \frac{\partial \mathcal{V}}{\partial T}\big|_P dT + \frac{\partial \mathcal{V}}{\partial P}\big|_T dP$, and using this in equation (5.18) gives

$$dQ = \left(C_V + L_V \frac{\partial \mathcal{V}}{\partial T}\bigg|_P \right) dT + L_V \frac{\partial \mathcal{V}}{\partial P}\bigg|_T dP. \tag{5.21}$$

Equating coefficients in equations (5.21) and (5.16) gives

$$C_P = C_V + L_V \frac{\partial \mathcal{V}}{\partial T}\bigg|_P \tag{5.22}$$

and

$$L_P = L_V \frac{\partial \mathcal{V}}{\partial P}\bigg|_T. \tag{5.23}$$

If the process is adiabatic, $dQ = 0$, we may eliminate dT in equation (5.20) and use equation (5.23) to find the ratio L_V/L_P. We thus obtain

$$\frac{dP}{d\mathcal{V}} = \frac{C_P}{C_V}\frac{L_V}{L_P} = \gamma \left.\frac{\partial P}{\partial \mathcal{V}}\right|_T. \tag{5.24}$$

Now $(\partial P/\partial \mathcal{V})_T$ is just the slope of the isotherm in the $P - \mathcal{V}$ plane. The adiabatic slope defined by equation (5.24), however, is greater by a factor of γ than the isothermal slope. The adiabatic index is defined as $\gamma \equiv C_P/C_V$, that is, it is the ratio of the material's specific heats. An ideal gas is defined as a gas consisting of a constant number N of non-interacting particles, and the specific heats are assumed to be constant. With these assumptions the solution of equation (5.24) yields

$$P\mathcal{V}^\gamma = \text{constant}. \tag{5.25}$$

We show in the next chapter that we can write the ideal gas equation of state as $P = NkT/\mathcal{V}$. Combining this with equations (5.19) and (5.25), we can write the equation of state for an ideal gas, in terms of the adiabatic index, as

$$\varepsilon = C_V T = \frac{1}{\gamma - 1} P\mathcal{V}. \tag{5.26}$$

Now, we can easily obtain the Hugoniot for an ideal gas by substituting equation (5.26) into equation (5.12) and rearranging:

$$\frac{P_1}{P_0} = \frac{(\gamma + 1)\,\mathcal{V}_0 - (\gamma - 1)\mathcal{V}_1}{(\gamma + 1)\,\mathcal{V}_1 - (\gamma - 1)\mathcal{V}_0}. \tag{5.27}$$

We may rearrange equation (5.27) to obtain the compression (density) ratio in the shocked ideal gas:

$$\frac{\rho_1}{\rho_0} = \frac{\mathcal{V}_0}{\mathcal{V}_1} = \frac{(\gamma + 1)\,P_1 + (\gamma - 1)P_0}{(\gamma - 1)\,P_1 + (\gamma + 1)P_0}. \tag{5.28}$$

From equation (5.28) we can clearly see that as the shock strength increases the compression does not increase indefinitely, but asymptotes to a particular limiting value that depends only on the adiabatic index. Thus, when $P_1 \gg P_0$, we may approximate equation (5.28) as

$$\frac{\rho_1}{\rho_0} = \frac{\gamma + 1}{\gamma - 1}. \tag{5.29}$$

The more degrees of freedom the individual particles of the gas have, the more ways there are for the energy to be partitioned, and the closer the two specific heats are to being equal. Thus, a diatomic gas in which vibrational modes are excited has an adiabatic index of $9/7$, so, by equation (5.29), its limiting shock compression

https://doi.org/10.1017/CBO9781139095150.005 Published online by Cambridge University Press

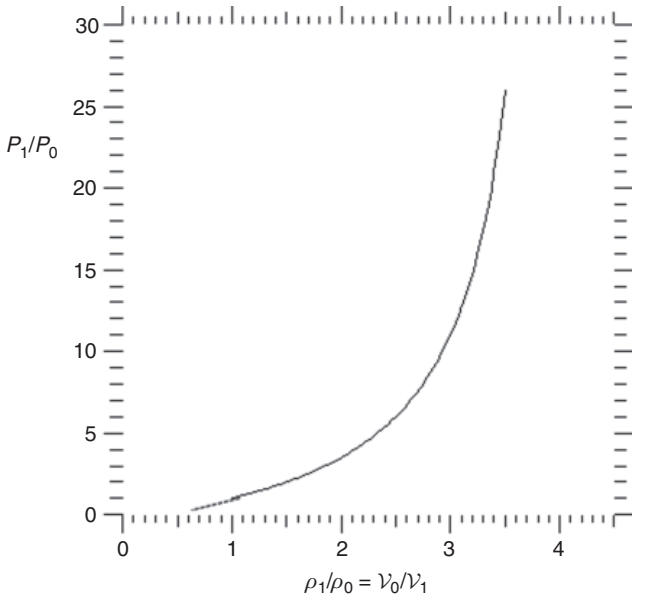

Figure 5.2 The Hugoniot curve for an ideal monatomic gas with initial conditions P_0 and $\mathcal{V}_0$.

ratio is 8. If the vibrational modes are not excited, then $\gamma = 7/5$, and the limiting compression ratio is 6.

In extreme conditions, where we are in general considering atoms that are not in molecular bonds, there are no vibrational and rotational modes, and the adiabatic index is larger, closer to that for a monoatomic ideal gas, $\gamma = 5/3$. Then, the limiting compression ratio, from equation (5.29), is 4. In actual plasmas at high temperatures, though, the specific heats and specific heat ratio are not constant, so equation (5.29) does not apply. Even in those cases, though, the compression does not increase without limit as the shock strength increases. As for an ideal gas, the compression limit is greater the higher the specific heats and the lower the adiabatic index.

The Hugoniot curve for an ideal monoatomic gas with initial conditions P_0 and $\mathcal{V}_0$ is shown in Figure 5.2. The curve to the left of the initial volume $\mathcal{V}_0$ is shown as a dashed curve to indicate that these Hugoniot states, which would be produced in a rarefaction shock, are physically unattainable, as we explained in Section 4.2.4. Rarefaction shocks are possible only under certain conditions for certain materials, when the rarefying material undergoes a phase transition as a result of the decompression, in which the new phase has a higher sound speed than the old phase. We will say more about shock-induced phase changes, and associated Hugoniots, in the next chapter.

Finally, let us examine the relationship between the flow velocities and shock velocity. First, we substitute the Hugoniot for an ideal gas, equation (5.28), into the equations for the flow velocities on either side of the shock, equations (5.10) and (5.11):

$$u_0^2 = \frac{\mathcal{V}_0}{2}\left[(\gamma-1)\,P_0 + (\gamma+1)P_1\right], \tag{5.30}$$

$$u_1^2 = \frac{\mathcal{V}_0}{2}\frac{\left[(\gamma+1)\,P_0 + (\gamma-1)P_1\right]^2}{\left[(\gamma-1)\,P_0 + (\gamma+1)P_1\right]}. \tag{5.31}$$

For strong shocks, when $P_1 \gg P_0$, we may approximate equations (5.30) and (5.31) as

$$u_0 = \left(\frac{\gamma+1}{2}P_1\mathcal{V}_0\right)^{1/2}, \tag{5.32}$$

$$u_1 = \left[\frac{(\gamma-1)^2}{2(\gamma+1)}P_1\mathcal{V}_0\right]^{1/2}. \tag{5.33}$$

Thus, the flow velocities on either side of the shock discontinuity increase as the square-root of the pressure.

Let us compare these flow velocities to the adiabatic sound speed. Combining equations (4.33) and (5.25) we find that the adiabatic sound speed in an ideal gas with constant specific heats is

$$c_s^2 = \left.\frac{\partial P}{\partial \rho}\right|_S = \gamma P \mathcal{V}. \tag{5.34}$$

Thus, combining equation (5.34) with equation (5.30), we find

$$\left(\frac{u_0}{c_{s0}}\right)^2 = \frac{(\gamma-1)+(\gamma+1)P_1/P_0}{2\gamma}. \tag{5.35}$$

Combining equation (5.34) with equation (5.31), and using equation (5.28), we find

$$\left(\frac{u_1}{c_{s1}}\right)^2 = \frac{(\gamma-1)+(\gamma+1)P_0/P_1}{2\gamma}. \tag{5.36}$$

Let us now consider two limiting cases:

1. In the limiting case of a weak shock, when $P_1 \approx P_0$, we see from equations (5.35) and (5.36) that $u_0 \approx c_{s0} \approx u_1 \approx c_{s1}$. Thus, a weak shock travels through the fluid ahead of it with a velocity that is close to the adiabatic sound speed. This is not surprising, since the adiabatic sound speed, as we saw in the last chapter, is the velocity at which small-amplitude acoustic disturbances propagate.

https://doi.org/10.1017/CBO9781139095150.005 Published online by Cambridge University Press

2. In the limiting case of a strong shock, when $P_1 \gg P_0$, we see from equation (5.36) that the flow velocity behind the shock will asymptote to a limiting value

$$u_1 = \left(\frac{\gamma - 1}{2\gamma}\right)^{1/2} c_{s1} < c_{s1}. \tag{5.37}$$

Indeed, for any shock, across which the flowing material is compressed, and thus $\mathcal{V}_1 < \mathcal{V}_0$ and $P_1 > P_0$, the material flowing into the shock is supersonic, that is, $u_0 > c_{s0}$, and the material flowing out of the shock is subsonic, that is, $u_1 < c_{s1}$.

All the above relations have been derived for a coordinate system in which the shock is stationary, so we considered that the material in front of the shock is flowing into it at velocity $-u_0$, while the material behind it is flowing out with velocity $-u_1$. If we now look at the same flow in a coordinate system in which the shock front moves at velocity u_s into stationary material (i.e., $u_0 = 0$), then, from the conservation of mass, equation (5.5), we find that the velocity of the shock discontinuity is

$$u_s = \frac{\rho_1}{\rho_1 - \rho_0} u_1. \tag{5.38}$$

Thus, from equation (5.37) we see that the shock velocity in an ideal gas cannot increase without limit. For weak shocks, $u_s \gg u_1$. Physically, this means that the shock moves well ahead of the "piston" push that created the shock. For strong shocks, on the other hand, $u_1 \approx u_s$. Physically, this means that the material behind the shock is set into motion at nearly the shock velocity. The ratio u_1/c_{s0} is called the Mach number of the shock. The Mach number is one way to characterize the strength of the shock. Another is, of course, the Hugoniot pressure, given in the case of an ideal gas by equation (5.27).

5.2 Shocks at boundaries and interfaces

5.2.1 Reflected shocks and Mach stems

Now let us consider the behavior of shocks at boundaries and at interfaces between different materials. In this subsection we first consider the behavior at a perfectly rigid boundary. In the next subsection we consider the behavior at non-rigid interfaces. The shock behavior is determined, as we shall see, by the relative shock impedances on either side of the boundary or interface. Shock impedance is the product of the material density and its adiabatic sound speed.

At a perfectly rigid boundary – a wall with infinite shock impedance – an incident shock will be fully reflected. That is, there is no transmitted shock into the wall.

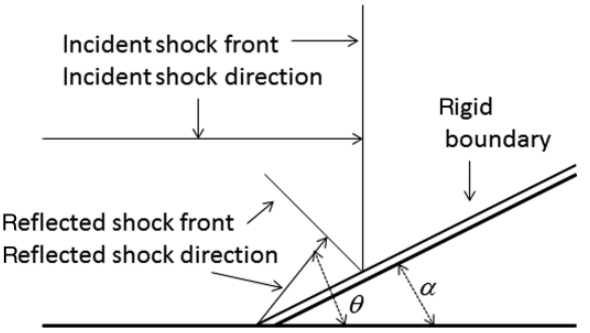

Figure 5.3 Geometry for reflection of a shock incident on a rigid boundary at an oblique angle.

A planar shock normally incident on a rigid boundary will reflect back on itself. Mathematically, this is equivalent to two equal-strength shocks moving in opposite directions and coming together at the position of the boundary. The conservation relations require that the material behind the reflected shock is stationary. The pressure behind the reflected shock, at least in the vicinity of the wall, is approximately twice the pressure behind the incident shock.

The situation for a shock obliquely incident on a rigid boundary is somewhat more complicated. Here, the behavior of the reflected shock, in particular the angle of the shock reflection, is a function of both the shock strength and the angle of incidence of the shock at the boundary.

The geometry for this situation is illustrated in Figure 5.3. The angle of incidence is α and the angle of reflection is θ. The Rankine–Hugoniot jump relations can be formulated, just as they were for the planar flow case in Section 5.1.1, but for this case they will include trigonometric functions of the two angles so as to account for continuity of the flow parallel to the boundary. We leave it as an exercise for the student to show that, for an ideal gas and for a given value of the shock strength P/P_0, we can determine θ, the angle of the reflected shock, from

$$P = P_0 + \rho_0 u_0^2 \sin^2\theta \left[1 - \frac{\tan(\theta - \alpha)}{\tan\theta}\right]. \tag{5.39}$$

For a given shock strength, oblique shock reflection can take one of two qualitatively different forms depending on the incidence angle, either regular reflection or Mach reflection.

Referring again to Figure 5.3, we see that any spatial position above the sloped boundary will experience two shocks in succession – the incident shock followed by the reflected shock. In regular reflection, which occurs when the incident shock is weak and/or when the incidence angle is not too large, the reflected shock along

https://doi.org/10.1017/CBO9781139095150.005 Published online by Cambridge University Press

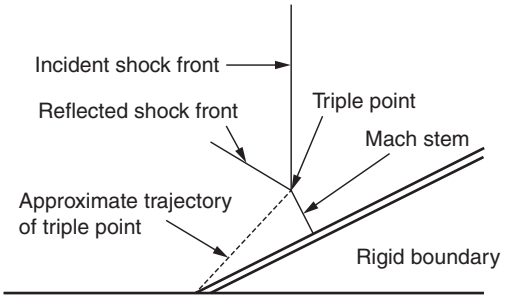

Figure 5.4 Schematic illustration of Mach reflection and Mach stem formation.

the rigid boundary always lags behind the incident shock. The circumstance where the reflected shock never overtakes the incident shock is regular reflection.

The reflected shock, however, always travels through material that has been heated and compressed by the incident shock. Thus, both the sound speed and shock velocity will be higher for the reflected shock than for the incident shock. If the incident shock is sufficiently strong and/or the incidence angle is sufficiently steep, the faster-moving reflected shock can overtake the incident shock. The region where the two shocks overlap is called the Mach stem, named for the German physicist who first observed this phenomenon. The point at which the incident, reflected, and merged shocks come together is called the triple point. Mach stem formation is illustrated schematically in Figure 5.4. As seen in this figure, the distance of the triple point from the rigid boundary increases with time as all three shocks propagate along the boundary. Thus, the amount of material contained within the region of the Mach stem grows with time.

5.2.2 Shocks at interfaces and the Richtmyer–Meshkov instability

The pressure jump behind a shock front can be written, from equation (4.49), as $\Delta P = \rho_0 c_{s0} u$. The product of the material's mass density and its adiabatic sound speed is called its shock impedance, that is, $Z = \rho c_s$. The shock impedance depends on the material's thermodynamic state conditions, and hence is different for different materials, and may possibly be different at different spatial positions in the same material.

At a boundary between materials with different shock impedances, some fraction of the incident shock energy will be reflected and the remainder of the incident shock energy will be transmitted across the interface, forming a new shock that propagates at a different velocity. If Z_1 is the shock impedance on one side of the interface, and Z_2 the shock impedance on the other side, with the shock propagating

from material 1 to material 2, then the pressure behind the reflected shock (i.e., the shock reflected back into material 1), P_R, is

$$\frac{P_R}{P_1} = \frac{Z_2 - Z_1}{Z_2 + Z_1}. \tag{5.40}$$

For a rigid boundary – the situation we discussed in the last subsection – the shock impedance of the rigid wall is infinite, so equation (5.40) says that all the shock energy is reflected back into material 1. At the other extreme, when the incident shock encounters an interface between two materials with nearly the same shock impedance, there is no reflected shock, or a very weak one; all or almost all the shock energy is transmitted across the interface into material 2.

The circumstance of a shock encountering a free surface will be discussed in the next subsection. First, we consider a shock incident on a perturbed interface between two fluids or plasmas with different shock impedances.

In Section 4.3.1 we derived the growth rate for the Rayleigh–Taylor instability. In the RT instability, perturbations on the interface between two different-density plasmas or fluids grow exponentially with time as the interface is accelerated in the direction of the denser material. The RT growth rate, equation (4.75), was derived by linearizing the conservation equations under the assumption that the perturbation amplitude is small compared to the wavelength of the perturbation, and that the acceleration of the interface is constant.

Perturbations on an interface can grow in amplitude also when the interface undergoes an acceleration that is not constant in time. A special case of non-constant acceleration is acceleration by a shock. We saw in Section 5.1.1 that the shock can be considered as a discontinuity in the flow, where the flow velocity discontinuously jumps by an amount $\Delta u = u_1 - u_0$. Thus, the acceleration can be represented by a delta function in the integration of the first term of the momentum conservation equation. That is, the first term of the momentum conservation equation, which is the partial derivative with respect to time of the momentum flux, can be written

$$\frac{\partial(\rho u)}{\partial t} = \rho \frac{\partial u}{\partial t} + u \frac{\partial \rho}{\partial t}, \tag{5.41}$$

and in the special case of a shock arriving at the interface at time t_0, we can directly integrate the first partial derivative in equation (5.41):

$$\int \rho \frac{\partial u}{\partial t} dt = \rho \int \frac{\partial u}{\partial t} \delta(t - t_0)\, dt = \rho \Delta u. \tag{5.42}$$

Here, $\delta(t - t_0)$ is the Kroenecker delta function, equal to one when $t = t_0$ and equal to zero otherwise.

We follow the same methodology we used in Section 4.3.1 to derive the growth rate for the classical RT instability – that is, we derive an equation of motion for the perturbation by linearizing the conservation equations under the assumption that in the initial linear growth phase of the instability the perturbation amplitude is small compared to the perturbation wavelength, and that the perturbation is incompressible. Now, for the shock acceleration case, we can directly integrate the equation of motion for the perturbation, using equation (5.42). We find that the perturbation grows linearly in time, rather than exponentially in time, with a growth rate

$$\gamma_{RM} = Ak\Delta u. \tag{5.43}$$

In equation (5.43) A is the post-shock Atwood number, defined in equation (4.76), and k is the wavenumber of the perturbation, defined in equation (4.64). The subscript on the shock-driven perturbation growth rate γ is meant to distinguish this growth rate from the classical buoyancy-driven RT perturbation growth rate given in equation (4.75). The shock-driven instability growth rate given in equation (5.43) was first derived by Richtmyer in 1960, expanding on the work of Taylor first published in 1950. The first experimental measurements of this instability growth were made by Meshkov in 1969. Hence, the shock-driven interface instability is often referred to as the Richtmyer–Meshkov instability.

For a given perturbation wavenumber the Richtmyer–Meshkov instability grows slower than the Rayleigh–Taylor instability, linearly in time rather than exponentially in time. When the amplitude of the perturbation, however, becomes comparable to the perturbation wavelength, the flow begins to become turbulent, with the generation of other wavenumber modes. The behavior of the turbulent mix layer is much like that described in Section 4.3.3. At the onset of non-linearity a material begins to lose memory of initial conditions. For fully developed turbulence all memory of initial conditions is lost.

In addition to the slower growth rate, there is another important difference between the Richtmyer–Meshkov and Rayleigh–Taylor instabilities. As we can see from equation (5.43), the absolute value of the perturbation amplitude can increase regardless of the sign of the Atwood number. In other words, it does not matter whether the shock is passing from the denser material to the less dense material or vice versa. In the latter case, as in the Rayleigh–Taylor instability, there is a monotonic increase in the perturbation amplitude. In the former case, the perturbation amplitude initially decreases, then reverses phase and grows linearly in time. Thus, a perturbation that is stable to classical Rayleigh–Taylor instability under the action of a constant acceleration in the direction of the less dense material will be unstable to shock acceleration in the same direction. In computer simulations

of the behavior of shock-driven matter, therefore, we cannot ignore the effects of shocks at interfaces and boundaries.

5.2.3 Emergence of shocks at a free surface

Finally, to conclude this section on the behavior of shock waves at boundaries and interfaces, let us consider the case where a planar shock is incident on a free surface, that is, an interface between a dense material and a vacuum. Let us assume that the pressure at the free surface is zero. This is the situation that obtains at the surface of a solid. Even if the solid is in air, the shock impedance of the highly compressible air is negligible compared to the shock impedance of the much less compressible solid, so the interface between the solid and the air can be considered, to a very good approximation, a free surface.

Let us further consider a "weak" planar shock propagating in the solid, with the shock front parallel to the free surface. In this instance, "weak" means that the shock is not strong enough to melt or vaporize the solid. It may, however, be strong enough to drive solid–solid phase transitions, which we will discuss in more detail in Section 6.3.3, and still be considered a weak shock. This is because most solids are not very compressible, that is, $\Delta\rho \ll \rho$ and $\Delta P \ll P$, so even shocks up to a few Mbar pressure can be considered as "weak," and thus the acoustic approximation we discussed in Chapter 4 applies. We further assume that the pressure behind the shock is large compared to the solid's material strength. We discuss material strength in more detail in Section 5.5. With this assumption we can, for now, ignore material strength, and the pressure can be considered isotropic, just as in a gas or liquid or plasma.

This "weak" shock propagates through the solid with a velocity approximately equal to the adiabatic sound speed in the unshocked material, c_{s0}. Then, the pressure jump behind the shock front can be written, using the acoustic approximation of equation (4.49), as $P = \rho_0 c_{s0} u$, where u is the material velocity behind the shock. At the time this shock emerges from the free surface, a rarefaction wave propagates back into the solid. As we saw in Chapter 4, the rarefaction wave travels backwards at an adiabatic sound speed which differs little from c_{s0}. Thus, the pressure across the shock wave at the instant of its emergence from the free surface drops from P to zero, that is, $\Delta P = -P$. Again, using the acoustic approximation, this pressure drop means that the material at the free surface acquires an additional velocity

$$u' = -\frac{\Delta P}{\rho_0 c_0} = \frac{P}{\rho_0 c_0} = u. \tag{5.44}$$

Thus, the material at the free surface is set into motion with a velocity approximately twice that of the velocity of the material behind the shock before it emerges from

the free surface. This velocity-doubling rule, even though an approximation, is quite accurate. Of course, the stronger the shock the less accurate is the velocity-doubling rule. Measurements have shown, though, that the rule is accurate to within about 2% for most metals up to as high as Mbar pressure. Thus, measurements of free surface particle velocities can provide a reasonably accurate determination of shock strengths.

The determination of shock strength by using equation (5.44) along with a measurement of the free-surface velocity depends, of course, on knowing the sound speed of the material. For weak shocks, the sound speed can be measured by measuring the difference in the emergence time of the shock from different thicknesses of the material. That is, identical shock waves are launched in two side-by-side identical foils of different thicknesses, and the sound speed is just the difference in thicknesses divided by the difference in the measured shock emergence times. The interaction of a very weak shock or an isentropic compression wave with the free surface, however, leads to very large errors in estimating the emergence time for these very slowly rising velocity–time profiles. In this circumstance, one can backwards integrate equation (5.44), that is, integrate $dP = \rho_0 c_{s0}(u)\,du$ to determine the particle velocity in the body of the material, or, alternatively, use the method of characteristics. These methods are used to determine equations of state, and are described in detail in references listed in the Further Reading.

5.3 Structure of the shock front

5.3.1 Entropy and adiabaticity

At the beginning of this chapter we treated the shock as a discontinuity in the flow variables, that is, we considered that the shock front had zero width. In this way we were able to apply the conservation laws for mass, momentum, and energy to derive the Hugoniot jump conditions that relate the flow variables behind the shock to the flow variables in front of the shock.

The implicit assumption in that derivation is that the shock compression process is adiabatic. That is, conservation of entropy also applies, so $dS/dt = 0$ across the shock discontinuity, where S is the entropy.

The important point to understand here is that the jump conditions, dependent as they are only on the laws of conservation of mass, momentum, and energy, are true whether or not the flow is adiabatic. The entropy may change across the shock front and the flow variables behind the shock front will still be given by the Hugoniot jump conditions. In other words, the Hugoniot jump conditions relate the flow variables behind the shock to those in front of the shock independent of the width of the shock front. Within the narrow shock front is the transition layer

within which the flow variables transition from their values in front of the shock to their values behind the shock.

Let us now look in more detail at what happens to the entropy of a fluid or plasma as it is compressed by a shock wave. As an example, we consider an ideal gas.

We will show in the next chapter that we can write the equation for the entropy of an ideal gas as

$$S = C_V \ln\left(P\mathcal{V}^{\gamma}\right). \tag{5.45}$$

As in equation (5.25), $\gamma = C_P/C_V$ is the adiabatic index. Then, substituting equation (5.28) into equation (5.45) we find that the change in entropy of the fluid or plasma across the shock transition layer is

$$S_1 - S_0 = C_V \ln\left\{\frac{P_1}{P_0}\left[\frac{(\gamma-1)(P_1/P_0)+(\gamma+1)}{(\gamma+1)(P_1/P_0)+(\gamma-1)}\right]^{\gamma}\right\}. \tag{5.46}$$

Let us again consider two limiting cases:

1. In the limiting case of a weak shock, $P_1 \approx P_0$, and thus, from equation (5.46), $S_1 \approx S_0$. Weak shocks, therefore, are approximately adiabatic. There is little dissipation of energy across the shock front of a weak shock.
2. For a very strong shock, where $P_1 \gg P_0$, the change in entropy across the shock transition layer is

$$S_1 - S_0 \approx C_V \ln\left\{\frac{P_1}{P_0}\left(\frac{\gamma-1}{\gamma+1}\right)^{\gamma}\right\}. \tag{5.47}$$

Thus, the entropy increases logarithmically with the shock strength. The entropy becomes infinite as the shock strength becomes infinite.

5.3.2 Viscosity and heat conduction

The increase in entropy across a shock transition layer means that irreversible dissipative processes are taking place in this transition layer. These dissipative processes take place at the atomic scale, in collisions between the particles comprising the fluid or plasma. The characteristic scale of the dissipation is therefore the relevant collisional mean free path.

Unless we wish to know the details of the physical processes that take place on this small scale in the fluid or plasma, there is no need to even know what dissipative processes take place in the shock in order to determine the macroscopic behavior of the flowing material. The dissipation processes on the macroscopic scale can be characterized by the material viscosity.

https://doi.org/10.1017/CBO9781139095150.005 Published online by Cambridge University Press

We can derive an expression for viscosity by considering the additional flux of momentum caused by the viscous processes in much the same way we derived the change in hydrodynamic momentum flux in Chapter 4. Let us consider a one-dimensional shock layer with a thickness on the order of the atomic or ionic collisional mean free path λ. The particles in this layer have an average thermal velocity of v_{th}. Then, the flux density of the total hydrodynamic momentum of the particles coming into the layer on one side is $\rho v_{th} u$. Similarly, the flux density of the total hydrodynamic momentum of the particles emerging from the other side of the layer is $v_{th}(u + \Delta u)$, where Δu is the change in the hydrodynamic velocity across the layer.

This additional momentum flux becomes an added term in the momentum conservation equation. Writing

$$\Delta u = \frac{\partial u}{\partial x}\lambda, \tag{5.48}$$

we can then rewrite the momentum conservation equation, equation (4.8), as

$$\frac{\partial}{\partial t}(\rho u) = -\frac{\partial}{\partial x}\left(P + \rho u^2 + \frac{4}{3}\mu\frac{\partial u}{\partial x}\right), \tag{5.49}$$

where μ, the shear viscosity coefficient, is defined as

$$\mu = \rho v_{th}\lambda, \tag{5.50}$$

and the constant $4/3$ arises from a consideration of the three-dimensional thermal motion of the particles.

The kinematic viscosity is defined as $\nu = \mu/\rho$, and thus has units of length squared divided by time.

All the microphysics that describes the dissipative processes that take place in the shock front is folded in to the macroscopic viscosity. We saw in Chapter 2 how to determine particle thermal velocities and collision mean free paths. These quantities can be determined – or at least estimated – from kinetic theory and the Boltzmann equation. Once those quantities are determined they can then be substituted into equation (5.50) to determine the viscosity.

The added term in parentheses on the right-hand side of equation (5.49) has units of pressure. This term is the added viscous stress. Generalizing to three dimensions, the viscous stress is

$$\boldsymbol{\sigma} = \frac{4}{3}\mu\nabla\cdot\mathbf{u}. \tag{5.51}$$

Equation (5.51) says that the viscosity is proportional to the ratio of the viscous stress and the divergence of the flow velocity. It is, in some sense, a measure of the resistance to the ordered flow that results from the viscous dissipation processes.

A fluid or plasma in which the viscosity is constant is called a Newtonian fluid. In general, both the viscous stress and the coefficient of viscosity are tensors. Many plasmas at extreme conditions are non-Newtonian.

With viscosity present we must also alter the conservation of energy equation to account for the energy dissipated by the viscous stresses in the shock transition layer.

Considering the energy flux in just the same way we did above for momentum flux, we find that the energy conservation equation, equation (4.9), with the addition of viscosity becomes

$$\frac{\partial}{\partial t}\left(\rho\varepsilon + \frac{\rho u^2}{2}\right) = -\frac{\partial}{\partial x}\left[\rho u\left(\varepsilon + \frac{u^2}{2}\right) + Pu - \frac{4}{3}\mu u\frac{\partial u}{\partial x}\right]. \tag{5.52}$$

Note that the entropy increase across the shock, given by equation (5.46), does not depend at all on the thickness of the shock layer. The entropy increase depends only on the thermodynamic properties of the material and the strength of the shock. The thickness of the shock front depends only on the rate of the dissipative processes. This is analogous to the behavior of any physical system that is coming into equilibrium with its surroundings. For example, a hot chunk of material that is immersed in a large cooler bath will eventually cool to the temperature of the bath, independent of the physical mechanisms that transfer heat from the hot matter to the cooler bath. The physical mechanisms of heat transfer determine only the rate at which the hot material cools, not its final temperature.

Thus, the energy dissipation mechanism in the shock front determines only the gradients of the flow variables in the shock transition layer, not their initial or final states. The gradient in pressure, for example, is approximately

$$\frac{dP}{dx} \approx \frac{P_1 - P_0}{\lambda}, \tag{5.53}$$

with P_1 and P_0 determined from the conservation equations. In the absence of viscosity, that is, when λ goes to zero, the gradient becomes infinitely steep and the shock is a discontinuity. When the viscous dissipation processes have a long mean free path, as in a low-density plasma, for example, the shock front is thicker and the gradients more shallow.

In general, the characteristic width of the shock transition layer, which is approximately the collisional mean free path of the viscous dissipation processes at work in the transition layer, is much smaller than the characteristic scale over which the flow variables change, $\Delta x = c_s \Delta t$, where Δt is the time interval over which there are only very small changes in the flow variables. In a hydrodynamics simulation computer code, the zone sizes are typically chosen to be approximately equal to Δx, a distance which is referred to as the Courant scale. We will say much more

about this in Chapters 11 and 12. Thus, in a typical hydrodynamics simulation we do not follow the details of the microphysics in the shock front, because all of the microphysics is taking place on a subgrid scale, not resolved by the numerical simulation. Indeed, for strong shocks in particular, the gradients of the flow variables even across a single Courant zone containing the shock discontinuity are too steep for the numerical scheme to remain numerically stable, so it is customary to add in some "artificial" or numerical viscosity in order to smear out the shock front over several computational zones. We will discuss this in much more detail in Section 12.1.3. The numerical viscosity is typically much greater than the actual viscosity. Remember, however, that the viscosity has no effect on the final values of the flow variables behind the shock. These final values are determined entirely from the Hugoniot jump conditions, and are independent of the thickness of the shock transition layer and the physical processes taking place in that layer.

In addition to the viscous dissipation that takes place in the shock transition layer, there may also be transport of the energy by thermal conduction. Thus, we need to add yet another term to the energy conservation equation to account for thermal conduction. With thermal conduction, equation (5.52) becomes

$$\frac{\partial}{\partial t}\left(\rho\varepsilon + \frac{\rho u^2}{2}\right) = -\frac{\partial}{\partial x}\left[\rho u\left(\varepsilon + \frac{u^2}{2}\right) + Pu - \frac{4}{3}\mu u\frac{\partial u}{\partial x} - \chi\frac{\partial T}{\partial x}\right], \quad (5.54)$$

where χ is the material thermal conductivity. In plasma we must write separate equations for the electrons and ions. Indeed, electron thermal conduction and ion thermal conduction are critical processes that must be taken into account in determining the flow variables. Thermal conduction is discussed in detail in Chapter 8.

Finally, for very strong shocks in which the radiation energy density is non-negligible, transport of energy into and out of the shock transition layer by radiation may be important. Indeed, since in some situations some of the photon mean free paths in the unshocked material can be large compared to the thickness of the shock transition layer, radiative heating of the material ahead of the shock can alter the conditions of the matter through which the shock is propagating. We will discuss radiation transport in more detail in Chapter 9, including a consideration of radiation-dominated hydrodynamics.

5.4 Blast waves

We now consider a special case of a very strong shock. Let us consider the radially expanding shock wave produced by the sudden release of some large amount of energy E into a small volume, as in an explosion. Let us further consider that the shock at times t after the time of the energy release t_0 has propagated to some radius

R that is large compared to the original radius of the energy deposition volume. Then, we can, to a high degree of accuracy, consider that the energy release took place instantaneously and at a single point in space. With this assumption we can then, using dimensional scaling arguments, determine the motion of the shock and the fluid behind the shock. We will find that the motion is determined solely by the explosion energy, and the initial density and thermodynamic characteristics of the fluid into which the shock is propagating.

This problem was first considered and solved by Sedov in 1946 (see the references listed in the Further Reading), so the point-source shock is referred to as the Sedov blast wave. These blast waves are produced by chemical and nuclear explosions in the atmosphere and by supernova explosions in the interstellar gas. They can also be produced by laser light deposition.

At the time the Sedov blast wave has reached a radius R, contained within the volume behind the blast wave is a mass of fluid

$$M = \frac{4}{3}\pi R^3 \rho_0, \tag{5.55}$$

a mass that is much larger than the mass of the original explosion products or the mass contained within the original energy deposition region. The pressure right behind the blast wave is approximately equal to the energy density in this shocked fluid, so $P \approx E/R^3$. Thus, the shock velocity scales as

$$u_s \sim u_1 \sim \left(\frac{P}{\rho}\right)^{1/2} \sim \left(\frac{E}{\rho_0}\right)^{1/2} \frac{1}{R^{3/2}}. \tag{5.56}$$

Here, u_1 is the material velocity behind the blast wave, which, as we see in equation (5.38), is approximately equal to the shock velocity for a very strong shock.

The shock velocity, however, can also be written as the time rate of change of the shock radius,

$$u_s = \frac{dR}{dt}. \tag{5.57}$$

Now, combining equations (5.56) and (5.57), we find that

$$t = a_0^{-5/2} \left(\frac{E}{\rho_0}\right)^{-1/2} R^{5/2}, \tag{5.58}$$

where a_0 is a constant of the integration.

Rearranging equation (5.58) we find

$$R = a_0 \left(\frac{E}{\rho_0}\right)^{1/5} t^{2/5}. \tag{5.59}$$

https://doi.org/10.1017/CBO9781139095150.005 Published online by Cambridge University Press

Thus, the Sedov blast wave expands in radius as the two-fifths power of time, and the absolute value of the radius is parameterized by the energy driving the wave and the initial density of the fluid through which it is propagating. Indeed, measurements of the radius–time behavior of a Sedov blast wave can be used to infer the energy that created the wave. High-speed optical framing camera records were used as the default method for determining the yield of atmospheric nuclear explosive tests.

Now, substituting equation (5.59) into equation (5.57), we find that the blast wave velocity scales with the blast wave radius as

$$u_s = \frac{2R}{5t} = \frac{2}{5} a_0^{5/2} \left(\frac{E}{\rho_0} \right)^{1/2} R^{-3/2}. \tag{5.60}$$

We see from equation (5.60) that the blast wave velocity, like its radius, is parameterized by the energy driving the wave. The wave velocity, however, decreases as the wave expands and sweeps up more and more of the ambient fluid in front of it. At some time the blast wave velocity will fall to a value at which the strong shock approximation no longer applies, so the solution outlined here is no longer valid.

Now let us determine a value for the constant a_0. We can estimate a value for this constant by considering that the blast wave basically plows up all the matter in front of it into a thin layer. The thickness of this layer, Δr, is small compared to the blast wave radius. We assume that all the mass that was initially contained in the spherical volume of radius R is now contained in the annular volume of thickness Δr at radius R, that is,

$$\frac{4}{3} \pi R^3 \rho_0 = 4\pi R^2 (\Delta r) \rho_1. \tag{5.61}$$

Thus,

$$\Delta r = \frac{R}{3} \frac{\rho_0}{\rho_1}. \tag{5.62}$$

For an ideal gas, we can use equation (5.29) to rewrite equation (5.62) as

$$\Delta r = \frac{R}{3} \frac{(\gamma - 1)}{(\gamma + 1)}. \tag{5.63}$$

For a strong shock in a monatomic fluid, $\Delta r = R/12$. Of course, air is not monatomic. Furthermore, in the presence of a strong shock the adiabatic index of air is not constant, since the shock can disassociate the molecules. Nonetheless, it is a reasonable approximation to take $\gamma \approx 1.2$–1.3 over much of the range of the Sedov blast wave in air. Thus, the thickness of the blast wave in air is $\Delta r \approx 0.03R$–$0.04R$.

Now, let us consider that behind this blast wave is a pressure P_1 given by the Hugoniot jump condition for a strong shock. It is the blast wave that is pushing this layer of fluid forward. At the front of the blast wave the pressure on the back side of the plowed-up fluid layer, pushing it along, is some fraction f of P_1. Thus, by Newton's second law, we can write

$$\frac{d}{dt}(Mu_1) = 4\pi R^2 f P_1. \tag{5.64}$$

Substituting into equation (5.64) the strong-shock jump conditions for u_1 and P_1, along with the mass M from equation (5.55), equation (5.64) can be rewritten as

$$\frac{1}{3}\frac{d}{dt}\left(R^3 u_s\right) = f R^2 u_s^2. \tag{5.65}$$

Expanding the derivative on the left-hand side of equation (5.65), and recalling that $dR/dt = u_s$, we can then rewrite equation (5.65) as

$$\frac{1}{3}R^3 u_s \frac{du_s}{dR} = (f-1)\, R^2 u_s^2. \tag{5.66}$$

Now, substituting equation (5.60) for u_s into equation (5.66), we find that $f = 1/2$. Thus, our thin-layer approximation tells us that the pressure pushing the layer outward is half the pressure behind the blast wave. If we were to get a more exact solution of the equations of motion by following the integral method of Sedov, we would find that f is actually a function of the adiabatic index γ; especially for smaller values of γ the approximate solution is a reasonably accurate approximation of the exact solution.

Now, we can write the total energy driving the blast wave as the sum of the internal energy and the kinetic energy of the thin layer:

$$E = \frac{1}{(\gamma-1)} \cdot \frac{4}{3}\pi R^3 \cdot f P_1 + M\frac{u_1^2}{2}. \tag{5.67}$$

Substituting into equation (5.67) $f = 1/2$, the equations for P_1 and u_1 in the strong-shock approximation, and equation (5.60) for u_s, we can rewrite equation (5.67) as

$$E = \frac{4\pi}{3}\rho_0 \left[\frac{1}{\gamma^2-1} + \frac{2}{(\gamma+1)^2}\right]\left[\frac{2}{5}a_0^{5/2}\left(\frac{E}{\rho_0}\right)^{1/2}\right]^2. \tag{5.68}$$

Finally, we rearrange equation (5.68) to find the constant a_0:

$$a_0 = \left[\frac{75}{16\pi} \cdot \frac{(\gamma-1)(\gamma+1)^2}{3\gamma-1}\right]^{1/5}. \tag{5.69}$$

https://doi.org/10.1017/CBO9781139095150.005 Published online by Cambridge University Press

Thus, a_0 depends only on the thermodynamic properties of the material through which the blast wave propagates. For air with $\gamma \approx 1.2$, for example, we find from equation (5.69) that $a_0 \approx 0.89$. Using this value of a_0 in equation (5.59), for example, shows that the blast wave from an energy release of 10^{21} ergs – the approximate energy release in an explosion of 20 kt of high explosive – travels more than 700 m in just 2 s. At this time the air pressure just behind the blast wave is about 223 atm. After the passage of the blast wave, the pressure in the "swept out" cavity behind it drops abruptly.

Similarly, a high-intensity laser can be used to deposit energy into a small volume of material that then "explodes" and drives a blast wave into a surrounding low-density gas. A 20-kJ laser-driven explosion, for example, can drive a blast wave a distance of more than 8 m in air in just 2 s. Since blast waves are self-similar flows, one can, for example, design a laser experiment to simulate the blast wave produced in an interstellar gas cloud by a supernova explosion. Indeed, a blast wave is just one example of a self-similar flow. As we saw in Section 4.1.4, any hydrodynamic flow that is self-similar can be scaled and still maintain the same relationships between the flow variables.

5.5 Shocks in solids

5.5.1 Elastic–plastic behavior and material strength

When stressed sufficiently, crystalline solids exhibit plastic deformation. In plastic deformation, two blocks of crystal slip past each other along discrete slip planes, leading to a permanent deformation of the solid. Plastic deformation is, in a sense, like fluid flow, and can be represented mathematically by the same conservation equations as for hydrodynamic flow, but with an added term in the momentum conservation equation. In this section we will learn how to add elastic–plastic flow to the hydrodynamic equations of motion.

There is at least one important difference between fluid flow and plastic deformation. Plastic deformation results from the motion of lattice dislocations along the slip planes. Discrete blocks of the crystal between the slip planes remain largely undistorted. Further deformation occurs either by more movement of dislocations along the existing slip planes or by the formation of new slip planes. The microscopic carriers of the deformation are thus lattice dislocations, and their motion is largely constrained to lie in these slip planes. Viscous fluid flow, in contrast, differs from plastic deformation in a fundamental way. The microscopic carriers of flow in a fluid are not lattice dislocations – the fluid does not support a lattice structure – but the atoms or ions themselves. In a fluid, therefore, the flow is not constrained to lie in any particular planes.

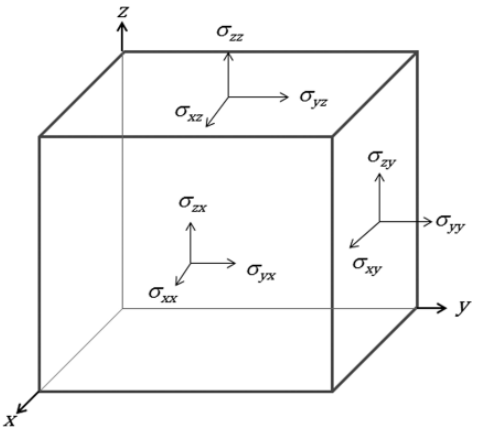

Figure 5.5 The stress tensor components.

Since a crystalline solid has a particular lattice structure, with spacing of the individual atoms that can be different in different lattice directions, the solid can have different mechanical properties in different lattice directions. This means that the solid does not, in general, respond isotropically to an applied force. The applied force, or pressure, is not isotropic in the material, but is instead described by a stress tensor. The deformation of the solid is then described by a strain tensor. The strain results from the application of the stress tensor. The components of the stress tensor are written as σ_{ij}, where the subscripts i and j denote the x, y, and z coordinate directions. The stress tensor is thus written as

$$\boldsymbol{\sigma} = \begin{vmatrix} \sigma_{xx} & \sigma_{yx} & \sigma_{zx} \\ \sigma_{xy} & \sigma_{yy} & \sigma_{zy} \\ \sigma_{xz} & \sigma_{yz} & \sigma_{zz} \end{vmatrix}. \tag{5.70}$$

Thus, σ_{ij} is the ith component of the stress acting on a unit area whose normal is in the jth coordinate direction. The normal components of the stress tensor are the diagonal elements of the tensor: σ_{xx}, σ_{yy}, and σ_{zz}. The other shear components are all the off-diagonal elements of the tensor, as illustrated in Figure 5.5. In general, the stress tensor is symmetric, so $\sigma_{ij} = \sigma_{ji}$.

The strain tensor $\boldsymbol{\varepsilon}$ likewise has nine components. When the deformation (strain) in any one direction is not too large, the solid responds elastically. That is, after the stress is removed, the atoms in the solid return to their initial positions as a result of the interatomic restoring forces holding the lattice structure together. In the elastic regime, Hooke's law applies, so the stress is directly proportional to the strain. For uniaxial strain in, say, the z-direction, Hooke's law is written as $\sigma_{zz} = E_z \varepsilon_{zz}$. Here, E_z is the elastic constant, or Young's modulus, in the z-direction.

https://doi.org/10.1017/CBO9781139095150.005 Published online by Cambridge University Press

Likewise, pure shear strain is linearly proportional to the shear stress, with a different constant of proportionality, G, the shear modulus. Any deformation can be decomposed into a sum of normal strains and shear strains.

Let us, for example, consider the uniaxial compression of a solid rod in the z-direction. For small deformation – that is, in the elastic regime – as the rod compresses in the z-direction, it expands in the lateral directions. The lateral expansion is proportional to the axial compression: $\varepsilon_{xz} = -\sigma\,\varepsilon_{zz}$, where σ is Poisson's ratio, another elastic property of the material, not to be confused with the stress. Since the overall volume in the compression cannot increase, it is easy to show that σ must always be less than or equal to $1/2$.

The other relevant mechanical property of the material is its bulk modulus, K. The bulk modulus is the reciprocal of the compressibility,

$$K = \rho_0 c_s^2, \tag{5.71}$$

where c_s is the adiabatic sound speed, given by equation (4.46). Thus, the bulk modulus is determined from the material equation of state, and characterizes the isotropic compressibility of the solid. As we discussed in Chapter 4, a solid is much less compressible than a gas, or even a liquid. A solid typically has a bulk modulus much greater than that of a gas or liquid. See, for example, the bulk moduli for Al and Fe, compared to that for hydrogen gas, in Appendix III.

The elastic properties of a solid are fully characterized by the four moduli E, G, σ, and K. Of course, the four moduli are not independent. They are connected by two relations. If we know any two of the moduli, we can determine the other two. For example, if we know Young's modulus and Poisson's ratio, we can determine the shear modulus and the bulk modulus from

$$G = \frac{E}{2(1+\sigma)} \tag{5.72}$$

and

$$K = \frac{E}{3\,(1-2\sigma)}, \tag{5.73}$$

respectively.

It is standard practice to decompose the stress tensor $\underline{\boldsymbol{\sigma}}$ into a mean pressure $P = (\sigma_{xx} + \sigma_{yy} + \sigma_{zz})/3$ and the deviatoric component:

$$\underline{\boldsymbol{\sigma}} = P\,\underline{\boldsymbol{I}} + \underline{\boldsymbol{\sigma}}_{dev}, \tag{5.74}$$

where $\underline{\boldsymbol{I}}$ is the identity tensor.

Assuming again a uniaxial compression in the z-direction, and a radially isotropic and homogeneous material, then $\sigma_{xx} = \sigma_{yy}$, and the shear stress σ_{zy} tangential to a

plane inclined at 45° to the axial direction is $\sigma_{zy} = (\sigma_{zz} - \sigma_{yy})/2$. Hence, the axial stress can be written as

$$\sigma_{zz} = P + \frac{4}{3}\sigma_{zy}. \tag{5.75}$$

The material yields and plastic deformation commences when the shear stress exceeds the shear strength, that is, when $\sigma_{zy} > \sigma^*_{zy}$, or when

$$2\sigma_{zy} = \left(\sigma_{zz} - \sigma_{yy}\right) > Y. \tag{5.76}$$

The stress σ^*_{zy} is the shear strength and Y is the yield strength of the material.

The relation (5.76) has general applicability. For the case of laterally unconstrained uniaxial compression, the normal stress in the axial direction, σ_{zz}, is the only component of the stress tensor – that is, all the other components are zero – so the plasticity criterion reduces to $\sigma_{zz} = P = Y$.

When the shear stress exceeds the shear strength, the material enters the plastic flow regime. That is, it no longer behaves elastically, so the deformation results in a permanent change in the shape of the material. In plastic flow, the excess elastic energy gained in the uniaxial compression is dissipated in the work done by the shear stress in the material, and the shear stress remains constant throughout the plastic flow. As the pressure becomes very large, $P \gg (4/3)\,\sigma_{zy}$, the material becomes more hydrostatic in character – that is, $\sigma_{zz} \approx \sigma_{xx} \approx \sigma_{yy}$. In plastic flow, the lattice keeps rearranging itself into a minimum energy state. The atoms "slide over" each other by dislocation generation and propagation, with a characteristic viscosity that depends on the stress and the strain rate. For a given volume, the elastic energy is a minimum if the compression is isotropic, preserving the lattice structure (in the absence of solid–solid phase transitions). The shear modulus, which in the plastic regime is proportional to $d\sigma_{zy}/d\varepsilon$, then goes to zero on a time scale characteristic of the motion of the lattice dislocations. This time scale is approximately equal to the interatomic spacing divided by the dislocation velocity, which is always less than the sound speed. The stress–strain curves for perfect plasticity in an isotropic solid are shown in Figure 5.6.

When the plastic strain is much larger than the elastic strain, in perfect plasticity the shear stress is proportional to the shear strain rate, that is, $\sigma_{ij} =$ (constant) $d\varepsilon_{ij}/dt$.

This relationship is identical in form to the relation between forces and motions in a viscous fluid, as in equation (5.51). For a Newtonian (constant kinematic viscosity ν) fluid, assuming the fluid is isotropic, we can write

$$\sigma_{ij} = 2\rho\nu\frac{d\varepsilon_{ij}}{dt}, \tag{5.77}$$

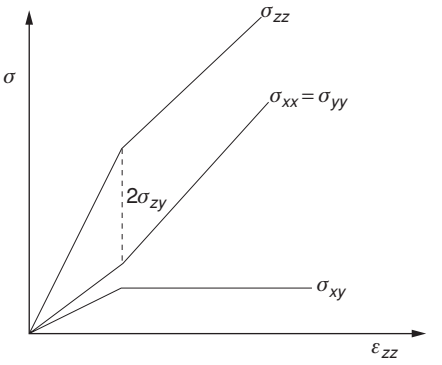

Figure 5.6 Stress–strain curves for axial compression of an isotropic solid.

where in the fluid case the "strain rate" is the velocity shear $\partial u_i/\partial x_j$. Thus, we can treat plastic flow as equivalent to viscous fluid flow, parameterized by an equivalent plastic viscosity. Furthermore, if we take the plasticity criterion first derived by von Mises in 1913 for perfect plasticity,

$$\left|\sigma_{ij}\right|^2 = \frac{2}{3}Y^2, \tag{5.78}$$

and then combine equations (5.77) and (5.78), we find the equivalent plastic kinematic viscosity that is consistent with the von Mises criterion:

$$\nu_{ep} = \frac{Y}{\sqrt{6}\rho\left|d\varepsilon_{ij}/dt\right|}. \tag{5.79}$$

The equivalent plastic viscosity of equation (5.79) defines the effective lattice viscosity for solid-state plastic flow. This expression was first derived in 2003 by one of the authors and co-workers, and is sometimes referred to as the Colvin equation. Owing to the very constrained nature of dislocation glide along specific slip planes in the crystalline solid, the effective lattice viscosity is typically many orders of magnitude larger than typical fluid viscosities, although some fluids – tree sap, for example – can have very large viscosities.

5.5.2 Material constitutive models

To account for the effects of material strength in the equations of motion describing shock propagation in a solid, we must replace the pressure in the pressure gradient term in the conservation of momentum equation with the stress tensor given by equation (5.74). This is the same thing as adding a term for the gradient of the

https://doi.org/10.1017/CBO9781139095150.005 Published online by Cambridge University Press

deviatoric stress. The deviatoric stress, of course, depends on the shear modulus G, equation (5.72), and reaches a limiting value that depends on the material strength Y. Both G and Y, in turn, depend on the material thermodynamic quantities pressure and temperature. In this sense the equations relating these quantities act just like equations of state in that we must have mathematical models for G and Y in order to solve the equations of motion for the behavior of the shocked solid. These mathematical models are the material constitutive models.

The material constitutive models, however, are much more complicated than equations of state, because in addition to G and Y depending on pressure and temperature, they also depend on strain rate, the particulars of the microstructure – grain sizes and orientations – of the material, the dynamical history of the material, and its original processing. Since plastic deformation results from the flow of lattice dislocations, not the motion of the atoms or ions themselves, as we discussed above, the presence and orientation of grain boundaries, which can inhibit dislocation motion, play a large role in determining material strength. Different microstructures result from different material processing and handling. Thus, two pieces of material that are otherwise identical chemically, and even identical in their lattice structure, may have very different constitutive properties as a result of different processing and handling. For example, wrought iron is microstructurally different from cast iron. An extruded Al rod is microstructurally different from a rolled sheet of Al.

Likewise, different dynamical histories can result in different constitutive properties. Even when two identical materials that have identical initial microstructures are subjected to shock loading, they may display different strength properties under different loading conditions.

For all these reasons, it has proven so far impossible to come up with a single constitutive model that describes plastic deformation for all materials under all loading conditions. This remains an area of vigorous research.

Constitutive models fall into two broad categories: phenomenological models and physically based models.

One phenomenological model that has seen widespread use is the constitutive model of Steinberg, developed by Dan Steinberg and co-workers in 1980. In the Steinberg model, the shear modulus and material strength are written as a Taylor series expansion in pressure and temperature, retaining only the first-order terms in the expansion, and setting the coefficients by fitting to dynamical data. Thus, the shear modulus and material strength are written as

$$G(P,T) = G_0 + G_P \frac{P}{\eta^{1/3}} - G_T (T - T_0) \tag{5.80}$$

https://doi.org/10.1017/CBO9781139095150.005 Published online by Cambridge University Press

and

$$Y(P,T) = \frac{Y_0 f\left(\varepsilon_p\right) G(P,T)}{G_0}, \tag{5.81}$$

where $\eta = \rho/\rho_0$ is the compressibility; the coefficients G_0, Y_0,

$$G_P = \left.\frac{\partial G}{\partial P}\right|_T = \text{constant}, \tag{5.82}$$

and

$$G_T = \left.\frac{\partial G}{\partial T}\right|_P = \text{constant} \tag{5.83}$$

are determined in fits to dynamical data; and f, a function of the plastic strain ε_p, describes the work hardening. The coefficients are given for Al and Fe in Appendix III.

In the Steinberg model, strength increases as the lattice potential energy increases – that is, as the atoms in the material are squeezed closer together – and decreases as the temperature increases. In general, though, the Steinberg model is applicable, if at all, only over a limited range of pressures and temperatures, and does not account for strain rate effects. Nonetheless, this model has been used with some success to model the dynamical behavior of a wide variety of materials under a wide variety of loading conditions.

Another widely used phenomenological model that does account for strain rate effects is the Johnson–Cook constitutive model, developed in 1983. In the Johnson–Cook model the material strength is written as

$$Y\left(\varepsilon_p, \dot{\varepsilon}_p, T\right) = \left(A + B\varepsilon_p^n\right)\left[1 + C\ln\left(\frac{\dot{\varepsilon}_p}{\dot{\varepsilon}_{p,0}}\right)\right]\left[1 - \left(\frac{T - T_0}{T_m - T_0}\right)^m\right]. \tag{5.84}$$

In equation (5.84), A, B, C, n, and m are the material-specific model coefficients; the argument of the logarithmic term is the dimensionless plastic strain rate for $\dot{\varepsilon}_{p,0} = 1\ \text{s}^{-1}$, and T_m is the melt temperature.

Note that, in the Johnson–Cook model, material strength goes to zero as the temperature approaches the melt temperature. This is an accurate description of the behavior of actual materials; a solid is a condensed material that has material strength, while a liquid is a condensed material that has no material strength. It is not the ordered lattice structure that defines the material as being solid. Some solids, including many alloys, are amorphous, so it is impossible to tell whether these materials are in a solid or liquid state just by looking at them with an electron microscope. Glass is one example of a common amorphous solid. At temperatures approaching the glass transition temperature the flow behavior of the glass can be modeled accurately as a very viscous liquid. Furthermore, some liquids, and

even some plasmas, can have an ordered structure. Rather than structure, then, it is presence or absence of material strength that distinguishes a solid from a liquid.

Note also that in the Johnson–Cook model the material strength increases both with increasing plastic strain and increasing plastic strain rate. This is also typical – but not necessarily universal – behavior of solids. The Johnson–Cook model says, however, that strength increases indefinitely as strain and/or strain rate go to infinity, and this limitless increase is not physically realistic. So, as for the Steinberg model, the Johnson–Cook model is, in general, applicable over only a limited range of strain and strain rate.

These two constitutive models – the Steinberg model and the Johnson–Cook model – are just two of some dozen or more constitutive models that have been developed for describing the behavior of dynamically compressed solids. Some of these other constitutive models are based on a physical picture of dislocation motion. It is beyond the scope of our discussion here to delve into the details of dislocation dynamics and constitutive models based on it. The student needs to be aware, however, that some prescription for material strength must be specified in simulating the behavior of shocked solids, and that it is not at all obvious *a priori* which prescription to pick. When we lack a definitive or universal model the thing to do is to start with a hypothesis for the model, design an experiment to test that hypothesis, then modify the model to better match the data from the experiment. Iterating this process is the very nature of the scientific method, and gets us closer and closer, in principle, to an accurate model.

Finally, we need to understand that constitutive models can tell us only how solids behave under compressive loads. Under tension, different material properties govern the behavior. In addition to material yield strength as discussed above, a solid has a tensile strength that is typically different from its yield strength. Once the tensile strength is exceeded, gaps, cracks, or voids may open up in the material. These cracks or voids can grow in size under the action of the stresses in the material. Coalescence of cracks and voids can result in material failure, that is, the solid breaking into pieces.

A common material failure that happens in shocked solids is spallation. We saw in Section 5.2.3 that when a shock wave emerges from a free surface, there is no reflected shock, and the material behind the incident shock expands. That is, a rarefaction wave travels backwards into the material from the free surface, moving at the adiabatic sound speed in the material.

Let us consider the situation where the incident shock was created by a pressure pulse driving the front surface of a solid foil. The compressed, higher-pressure material behind this shock as it propagates into the material drives a backward-propagating compression wave, which, when it emerges from the front free surface, launches a rarefaction wave that travels back into the material behind the shock.

When the shock finally travels across the whole thickness of the foil and emerges from the back free surface, it generates another counter-propagating rarefaction wave back into the material from that free surface. At the position in the material where the two counter-propagating rarefaction waves cross – a position that is typically not too far back from the back surface – the material at that position is in tension. That is, the material at that position is being pulled in both directions simultaneously. If the tensile stress at that position exceeds the tensile strength of the material, the layer of material between this position and the back surface spalls, or breaks off entirely from the rest of the foil. The spalled material will then continue to move away from the rest of the foil at the velocity it had at the time of spallation.

If, in contrast, the tensile stress at the crossing position of the rarefaction waves does not exceed the tensile strength of the material, the material remains in the elastic regime, and is "pulled back" to its original position and zero velocity. This suggests a way to measure tensile strengths of materials. By measuring the velocity history of the back surface of a solid that spalls, we can relate the difference between the peak velocity and the final velocity of the back surface to the pressure (equal to the tensile strength for an unconstrained unidirectional shock) using equation (5.44).

Materials with a low tensile strength are said to be ductile. This means that they can stretch and deform plastically to fairly high strains without breaking apart. Materials with a high tensile strength, however, are more brittle, which means that they will stretch more elastically until they break under the action of the elastic stresses. Many metals are ductile, while rocks tend to be brittle.

5.5.3 Solid-state Rayleigh–Taylor instability

To conclude our discussion of shocks in solids, let us now consider how perturbations on the surface of a solid grow as the solid is accelerated by a lower-density fluid. As we discussed in Chapter 4, the surface or interface being accelerated by the lower-density fluid is classically Rayleigh–Taylor unstable. Material strength, however, acts to reduce – and in some circumstances even to suppress completely – the classical inviscid fluid Rayleigh–Taylor growth rate given by equation (4.75). We address two questions: (1) where are the elastic limits below which perturbations do not grow, and on what properties of the material and the perturbations do they depend; and (2) when these elastic limits are exceeded and the material transitions to plastic flow, what is the solid-state Rayleigh–Taylor growth rate?

Let us address the first question first. We start by considering material-strength stabilization in two limiting cases. In the limit of zero initial perturbation amplitude,

a perturbation does not grow at all if the shear wave can transmit the restoring force of the lattice *across* the perturbation in less time than the characteristic growth time of the perturbation. We can write this condition as

$$\frac{1}{k\rho\sqrt{G}} < \frac{1}{\sqrt{kAa}}, \tag{5.85}$$

from which the cutoff wavelength for instability growth is determined:

$$\lambda_c = \frac{2\pi G}{Aa\rho}. \tag{5.86}$$

As before, k is the perturbation wavenumber, G is the material's shear modulus, a is the constant acceleration, ρ the material density, and A the Atwood number, given by equation (4.76). Equation (5.86) was first derived by Miles in 1966 and is thus called the Miles criterion.

In the limit of zero wavelength, the elastic limit in compression is exceeded when the differential stress *over* the perturbation of amplitude η exceeds the material yield strength Y. Thus, the critical amplitude for instability growth can be written as

$$\eta_c = \frac{Y}{2a\rho}, \tag{5.87}$$

modified by a multiplicative factor of order unity that accounts for the perturbation shape. Equation (5.87) was first derived by Drucker in 1980, and is thus called the Drucker criterion.

In actual materials, the threshold for instability growth depends on *both* the perturbation amplitude and its wavelength because of differential stresses and wave propagation in the driven solid. In 1993 Lebedev and co-workers derived an amplitude threshold for instability growth, η_{th}, that is a function of the perturbation wavelength and the thickness of the material, h, in the direction of the acceleration:

$$\frac{\eta_{th}}{\eta_c} = \left[1 - 0.86\exp\left(-\frac{2\pi h}{\lambda\sqrt{3}}\right)\right]\left\{\left[1 - \exp\left(-\frac{2\pi h}{\lambda\sqrt{3}}\right)\right]^2 - \left(\frac{\lambda}{\lambda_c}\right)^2\right\}. \tag{5.88}$$

Equation (5.88), for infinite-thickness solids, reduces to the Miles elastic limit, equation (5.86), in the limit of zero amplitude, and to the Drucker elastic limit, equation (5.87), in the limit of zero wavelength. For finite-thickness solids, $\eta_{th} = 0$ for some wavelength $\lambda < \lambda_c$ that depends on h/λ_c. Thus, some perturbations that have wavelengths less than the Miles cutoff wavelength and amplitudes less than the Drucker threshold amplitude can still grow unstably in the elastic deformation regime. Furthermore, the threshold for instability growth may also depend on the time variation of the pressure driving the acceleration. For example, shear-strength stabilization can be lost, even in the steady state, for wavelengths on the order of

the material thickness, when the perturbation grows above the critical amplitude during the time of pressure ramp-up. In that circumstance, the only effect of the material strength is to retard, not suppress, the perturbation growth.

As we have seen, once the critical shear stress in the material is exceeded, the material transitions to plastic flow, and the shear modulus goes to zero. Then, all perturbation wavelengths grow monotonically at a rate that depends on the wavelength and the equivalent plastic viscosity, equation (5.79).

Equivalent plastic viscosity acts in the solid case just like viscosity acts in the fluid case. We discussed how viscosity acts to reduce the classical fluid Rayleigh–Taylor instability growth rate in Section 4.3.2. The dispersion equation for Rayleigh–Taylor instability growth in a viscous fluid is written in equation (4.81). The analogous dispersion equation for Rayleigh–Taylor instability growth in a solid can be written as

$$\gamma_s^2 + 2k^2\nu_{ep}\gamma_s + k \cdot \tanh(kh) \cdot \left(\frac{kG}{\rho} - Aa\right) = 0. \tag{5.89}$$

The second term in equation (5.89) is the viscous or plastic flow term, the third is the elasticity term, and the fourth is the usual acceleration term for linear-regime Rayleigh–Taylor growth. The effects of finite thickness are accounted for through the hyperbolic tangent factor.

The solution of the second-order equation, equation (5.89), is

$$\gamma_s = \nu_{ep}k^2 \left\{ \left[1 - \left(\frac{C}{\nu_{ep}^2 k^3} \right) \right]^{1/2} - 1 \right\}, \tag{5.90}$$

where

$$C = \tanh(kh) \cdot \left(\frac{kG}{\rho} - Aa\right). \tag{5.91}$$

Equations (5.90) and (5.91) indicate that the perturbation is unstable and grows (i.e., $\gamma_s > 0$) only for $k < k_c$, or wavelength of the perturbation $\lambda > \lambda_c = 2\pi G/Aa\rho$, recovering the Miles limit in the elastic regime. Thus, for $\lambda > \lambda_c$ the perturbations can grow in the elastic regime. If the perturbation growth is very small – that is, if the amplitude stays small compared to the wavelength – this growth can occur as a nearly reversible process, and the effective lattice viscosity is small. If this growth continued to large amplitude, it would transition into the plastic flow regime, where $G = 0$, the effective lattice viscosity becomes significant, and the process is no longer reversible. In the fully plastic regime, when $G = 0$, all wavelengths grow at a rate reduced from classical as a result of the effective lattice viscosity.

5.6 Example problems and exercises

In doing these problems and exercises, the student can use the thermodynamic and material properties for select materials listed in Appendix III.

Exercise 5.1. Use equations (5.5) and (5.6) to derive equations (5.10) and (5.11).

Exercise 5.2. Derive equation (5.12).

Exercise 5.3. Derive equation (5.15).

Exercise 5.4. Replot Figure 5.2, the Hugoniot curve for an ideal monatomic gas, for a diatomic deuterium gas, including molecular vibrational modes in the adiabatic index.

Exercise 5.5. What is the limiting flow velocity compared to the sound speed behind a strong shock in a diatomic deuterium gas, including molecular vibrational modes in the adiabatic index?

Exercise 5.6. Derive equation (5.39).

Exercise 5.7. What is the strength of the reflected shock in solid aluminum relative to the incident shock on an interface between solid aluminum and solid iron?

Exercise 5.8. What is the free-surface velocity imparted by the emergence of a 1-Mbar shock from solid aluminum?

Exercise 5.9. What is the change in entropy across a 1-Mbar shock in STP diatomic deuterium gas, including molecular vibrational modes in the adiabatic index?

Exercise 5.10. Derive equation (5.58).

Exercise 5.11. Show that the pressure right behind a Sedov blast wave in an ideal gas is

$$P_1 = \frac{4}{5(\gamma + 1)} a_0^5 \frac{E}{R^3}.$$

Exercise 5.12. Consider two different explosions in air. At time t after the first explosion the radius of the blast wave is measured to be R_1. At the same time t after the second explosion the radius of the blast wave is measured to be $R_2 = R_1/2$. What is the energy of the second explosion relative to that of the first?

Exercise 5.13. What is the elastic wave speed and the shear wave speed in 1100 Al, and how do these speeds compare to the bulk sound speed?

Exercise 5.14. Lasers are particularly useful for creating high-strain-rate shocks in solids. Strain rates up to 10^9 s^{-1} can be achieved. At this strain rate, what is the effective lattice viscosity in STP Al? How does this compare with the viscosity of water? How does it compare with the viscosity of cold cream (glycerin)?

Exercise 5.15. Using the Steinberg constitutive model, what is the shear modulus of 1100 Al compressed by a 100-kbar shock? *Hint:* Find the compression from the shock Hugoniot of Al shown in Figure 5.1, and assume no thermal softening.

Exercise 5.16. Does a 10-kbar shock exceed the yield strength of 1100 Al? Does a 100-kbar shock exceed the yield strength?

Exercise 5.17. Plot the Johnson–Cook yield strength as a function of plastic strain rate, ignoring thermal softening, for Fe shock-deformed to 10% strain.

Exercise 5.18. Plot the normalized perturbation amplitude threshold, η_{th}/η_c, versus the normalized perturbation wavelength cutoff, λ/λ_c, for solid-state Rayleigh–Taylor instability growth for $h/\lambda_c = \infty$, 0.25, and 0.05.

Exercise 5.19. Using the effective lattice viscosity for Al determined in Exercise 5.14, determine the Rayleigh–Taylor growth rate for a 100-μm wavelength sinusoidal perturbation on the surface of a 0.5-mm-thick Al foil driven by a pressure pulse of 100 kbar in 2 ns.

Exercise 5.20. For the problem of Exercise 5.19, at what time after the start of the Rayleigh–Taylor instability does the perturbation growth become non-linear (i.e., when does the amplitude become comparable to the wavelength) for an initial amplitude of 2 μm?